CRYSTAL GROWTH & DESIGN

Article

pubs.acs.org/crystal

Rectangle versus Square Oxalate-Connective Tetralanthanide Cluster Anchored in Lacunary Lindqvist Isopolytungstates: Syntheses, Structures, and Properties

Junwei Zhao,*[†,‡] Hailou Li,[†] Yanzhou Li,[†,‡] Chunyang Li,[§] Zhenling Wang,*[§] and Lijuan Chen*[†]

[†]Henan Key Laboratory of Polyoxometalate Chemistry, Institute of Molecular and Crystal Engineering, College of Chemistry and Chemical Engineering, Henan University, Kaifeng, Henan 475004, People's Republic of China

[‡]State Key Laboratory of Structural Chemistry, Fujian Institute of Research on the Structure of Matter, Chinese Academy of Sciences, Fuzhou, Fujian 350002, People's Republic of China

[§]Henan Key Laboratory of Rare Earth Functional Materials and Applications, Zhoukou Normal University, Zhoukou, Henan 466001, People's Republic of China

Supporting Information

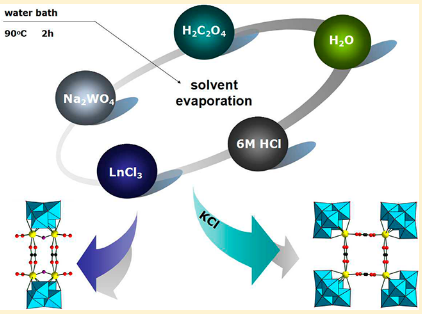

ABSTRACT: Two types of unique oxalate-connective lanthanide-substituted isopolyoxotungstates, $Na_{10}[Ln_2(C_2O_4)(H_2O)_4(OH)W_4O_{16}]_2\cdot 30H_2O$ (**1**) and $K_4Na_{16}[Ln(C_2O_4)W_5O_{18}]_4\cdot 60H_2O$ (**2**) (Ln = Eu^{III}, Ho^{III}, Er^{III}, or Tb^{III}), have been synthesized under conventional aqueous solution conditions and structurally characterized by elemental analyses, IR spectra, single-crystal X-ray diffraction, and thermogravimetric analyses. It should be pointed out that the utilization of different alkaline cations leads to the formation of two structural types. When only Na^+ ions are present in the system, type **1** was obtained, while when Na^+ and K^+ ions are used, type **2** was found. Complex **1** is a double-oxalate-bridging di-Ln substituted Lindqvist dimer with a rectangle tetra-Ln cluster, whereas **2** is a single-oxalate-connective mono-Ln^{III} Lindqvist tetramer with square tetra-Ln cluster. As far as we know, such di-Ln substituted Lindqvist fragment in **1** is observed for the first time. Moreover, **2** represents the first organic−inorganic hybrid square Ln-substituted isopolyoxotungstate. The solid-state luminescent properties of **1-Eu**, **1-Tb**, **2-Eu**, and **2-Tb** have been measured. **1-Eu** and **2-Eu** display intense, sharp, and narrow emission bands in the orange visible region that originate from the characteristic $^5D_0 \rightarrow {}^7F_J$ transitions, and their fluorescence lifetimes are 1.18 and 1.20 ms, respectively. **1-Tb** and **2-Tb** exhibit green photoluminescence mainly derived from $^5D_4 \rightarrow {}^7F_5$ transitions. The decay behavior of **1-Tb** can be fitted to a biexponential function with lifetimes of $\tau_1 = 0.43$ ms and $\tau_2 = 1.25$ ms, whereas the decay behavior of **2-Tb** can be fitted to single exponential function with the lifetime of 1.03 ms. Magnetic susceptibilities of **1** and **2** have been measured, and the decline of $\chi_M T$ upon cooling for **1** and **2** is mostly related to the progressive thermal depopulation of the excited state of Ln cations.

INTRODUCTION

The current increasing interest in the design and synthesis of inorganic−organic hybrid materials not only stems from abundant electronic configurations and bonding patterns in sophisticated structures but also is because interactions between organic and inorganic components can generate special phenomena of fundamental and practical interest in catalysis, molecular magnetism, gas sorption, and optical and electronic materials.[1] In this context, polyoxometalates (POMs), as intriguing metal−oxygen anionic clusters, can function as multidentate inorganic ligands to bind most of transition-metal (TM) and lanthanide (Ln) cations forming special functional hybrid materials that are derived from their controlled physical and chemical properties at the atomic and molecular levels and the synergistic effects between POMs and organic components.[2] In the POM field, an emerging topic has drawn enormous attention to the design and preparation of novel carboxylate-based TM/Ln substituted POM hybrids with unique optical, magnetic, and catalytic properties, since an attractive strategy was first reported by Dolbecq et al. in 2003, which involved using the prefabricated ε-Keggin precursor $[\varepsilon\text{-}PMo_{12}O_{36}(OH)_4\{La(H_2O)_4\}_4]^{5+}$ to react with carboxylates to prepare hybrid POMs.[3] The potential of this synthetic approach has afforded a class of POM hybrids with various stoichiometries and symmetries.[4] For example, in 2004, the acetate-bridging $[\{Ln(\alpha\text{-}SiW_{11}O_{39})(H_2O)_2\}_2(\mu\text{-}CH_3COO)_2]^{12-}$ (Ln = Eu^{III}, Gd^{III}, or Yb^{III}) dimers were obtained in CH_3COOH−CH_3COOK buffer.[4a] Concomitantly, Kortz reported a similar Dawson-type species, $[\{La(\alpha_2\text{-}P_2W_{17}O_{61})(H_2O)_2\}_2(\mu\text{-}CH_3COO)_2]^{16-}$.[4b] In 2008, several POM−organic frameworks (POMOFs) based on $\{Ni_6PW_9\}$ units and rigid carboxylate connectors were prepared by Yang

Received: May 7, 2014
Revised: September 22, 2014
Published: October 3, 2014

et al.[4c] Later, Liu's group synthesized a family of stable crystalline catalysts $[Cu_2(BTC)_{4/3}(H_2O)_2]_6[H_nXM_{12}O_{40}]\cdot(C_4H_{12}N)_2$ (X = Si, Ge, P, or As; M = W or Mo; BTC = benzenetricarboxylate).[4d] A redox active POMOF, $[NBu_4]_3[PMo^V_8Mo^{VI}_4O_{36}(OH)_4Zn_4(BDC)_2]\cdot 2H_2O$ (NBu_4 = tetrabutylammonium, BDC = benzenedicarboxylate), and a family of POMOF catalysts for hydrogen evolution were communicated by Dolbecq et al.[4e,f] In 2013, several di-Pd substituted γ-Keggin POMs with variable-length organic connectors, $TBA_8[\{(\gamma\text{-}H_2SiW_{10}O_{36}Pd_2)(O_2C(CH_2)_nCO_2)\}_2]$ (n = 1, 3, or 5; TBA = tetrabutylammonium) was reported by Mizuno and coworkers.[2e]

It is very conspicuous that all above-mentioned hybrids are carboxylate-based heteropolyoxotungstates or -molybdates, most of which were synthesized by means of POM precursors. Furthermore, the synthetic processes are multistep. However, is it probable that the self-assembly reaction of simple tungstates with Ln cations with the participation of functional polycarboxylates under usual bench conditions can prepare novel carboxylate-based Ln substituted isopolyoxotungstate hybrids. In such a one-step reaction, it is unnecessary to synthesize POM precursors, which can significantly shorten the experiment process. To the best of our knowledge, there is no relevant report, especially for Ln-substituted lacunary Lindqvist POM derivatives, which provides us an excellent opportunity. In this background, recently, we have launched the exploration on the system including sodium tungstate, Ln salts, and polycarboxylate ligands through a one-step procedure on the basise of the following ideas: (i) the acidic aqueous media was selected because this environment is beneficial to the polymerization of isopolyoxotungstates, can effectively reduce the precipitation of Ln elements, and greatly improves the reaction activity between isopolyoxotungstates and Ln−polycarboxylate complexes; (ii) highly oxyphilic Ln electrophiles can work as structure-stabilizing agents by their coordination mode to enhance the stability of in situ formed isopolyoxotungstates; (iii) electron-conjugated polycarboxylate chromophores and POM fragments not only can act as sensitizers of Ln luminescence in Ln-POMs through the "antenna effect"[5] but can integrate Ln cations together to construct novel magnetic aggregates or extended frameworks. In this avenue, two types of unprecedented oxalate-bridging tetra-Ln substituted Lindqvist isopolyoxotungstates, $Na_{10}[Ln_2(C_2O_4)(H_2O)_4(OH)W_4O_{16}]_2\cdot 30H_2O$ (**1**) and $K_4Na_{16}[Ln(C_2O_4)W_5O_{18}]_4\cdot 60H_2O$ (**2**) (Ln = Eu^{III}, Ho^{III}, Er^{III}, or Tb^{III}), were first separated. Interestingly, the use of different alkaline cations leads to the formation of two structural types. When only Na^+ ions are present in the reaction, type **1** was obtained, while when Na^+ and K^+ ions are used, type **2** was formed. **1-Eu** and **2-Eu** display strong orange fluorescence, while **1-Tb** and **2-Tb** exhibit green photoluminescence. Notably, the emission modes of **1-Eu**, **2-Eu**, **1-Tb**, and **2-Tb** all involve POM-centered ligand-to-metal charge-transfer (LMCT) processes, as well as a weak contribution of oxalate ligands. Magnetic properties of all complexes **1** and **2** have been investigated. No frequency dependence of the alternating current magnetic susceptibilities for **1-Ho**, **1-Er**, **1-Tb**, **2-Ho**, **2-Er**, and **2-Tb** suggests the absence of slow relaxation of the magnetization.

EXPERIMENTAL SECTION

Materials and Methods. All chemicals were commercially purchased and used without further purification. Carbon and hydrogen elemental analyses were performed on a Perkin−Elmer 2400-II CHNS/O analyzer. Inductively coupled plasma atomic emission spectrometry (ICP-AES) was carried out on a Perkin−Elmer Optima 2000 ICP-AES spectrometer. IR spectra were recorded from solid samples palletized with KBr on a Nicolet 170 SXFT−IR spectrometer in the range 400−4000 cm^{-1}. Photoluminescence spectra and lifetime were recorded using an FLS 920P Edinburgh Analytical Instrument apparatus equipped with a 450 W xenon lamp and a μF900H high-energy microsecond flashlamp as the excitation sources. Magnetic measurements were conducted on a Quantum Design MPMS XL-7 magnetometer in the temperature range of 2−300 K. The magnetic susceptibility data were corrected from the diamagnetic contributions as deduced by using Pascal's constant tables. Thermogravimetric (TG) analyses were performed under a N_2 atmosphere on a Mettler−Toledo TGA/SDTA 851^e instrument with a heating rate of 10 °C min^{-1} from 25 to 700 °C.

Syntheses of $Na_{10}[Ln_2(C_2O_4)(H_2O)_4(OH)W_4O_{16}]_2\cdot 30H_2O$ (1) (Ln = Eu^{III}, Ho^{III}, Er^{III}, or Tb^{III}). $Na_2WO_4\cdot 2H_2O$ (2.43 g, 7.37 mmol) and oxalic acid (0.063 g, 0.70 mmol) were dissolved in water (20 mL) under stirring. The pH of the solution was adjusted to 7.5 using HCl (6 $mol\cdot L^{-1}$). After 20 min stirring, $EuCl_3$ (0.25 g, 0.97 mmol), $HoCl_3$ (0.25 g, 0.92 mmol), $ErCl_3$ (0.25 g, 0.91 mmol) or $TbCl_3$ (0.25 g, 0.94 mmol) was added to the solution. After another 30 min continuous stirring, the resulting solution was kept at 90 °C in a water bath for 2 h and then cooled to room temperature and filtered. Slow evaporation at room temperature resulted in colorless square lamellar crystals for **1-Eu**, light yellow square flaky crystals for **1-Ho**, pink square lamellar crystals for **1-Er**, or colorless square lamellar crystals for **1-Tb** after about 1 week, which were filtered off and air-dried. Yield: 0.27g (30%) for **1-Eu**, 0.31 g (36%) for **1-Ho**, 0.33 g (38%) for **1-Er**, and 0.29 g (33%) for **1-Tb** based on $LnCl_3$. Elemental analysis (%) calcd for **1-Eu**: H, 2.22; C, 1.29; Na, 6.18; Eu, 16.34; W, 39.54. Found: H, 1.96; C, 1.34; Na, 6.07; Eu, 16.47; W, 39.40. Elemental analysis (%) calcd for **1-Ho**: H, 2.19; C, 1.27; Na, 6.10; Ho, 17.49; W, 39.00. Found: H, 2.06; C, 1.29; Na, 5.89; Ho, 17.61; W, 39.22. Elemental analysis (%) calcd for **1-Er**: H, 2.19; C, 1.27; Na, 6.08; Er, 17.70; W, 38.90. Found: H, 2.02; C, 1.29; Na, 6.22; Er, 17.55; W, 38.76. Elemental analysis (%) calcd for **1-Tb**: H, 2.21; C, 1.28; Na, 6.14; Tb, 16.97; W, 39.25. Found: H, 2.39; C, 1.37; Na, 5.98; Tb, 17.22; W, 39.08. IR (KBr, cm^{-1}): 3432s, 1655s, 1320m, 940s, 838s, 789s, 677s, 584w, 538m, 476w, 431w for **1-Eu**; 3436s, 1663s, 1320m, 940s, 837s, 784s, 681s, 592w, 543m, 480w, 435w for **1-Ho**; 3440s, 1665s, 1324m, 941s, 838s, 788s, 681s, 592w, 544m, 486w, 432w for **1-Er**; 3438s, 1666s, 1328m, 939s, 836s, 798s, 682s, 585w, 547m, 489w, 431w for **1-Tb**.

Syntheses of $K_4Na_{16}[Ln(C_2O_4)W_5O_{18}]_4\cdot 60H_2O$ (2) (Ln = Eu^{III}, Ho^{III}, Er^{III}, or Tb^{III}). $Na_2WO_4\cdot 2H_2O$ (2.43 g, 7.37 mmol), oxalic acid (0.063 g, 0.70 mmol), and KCl (0.20 g, 2.68 mmol) were dissolved in water (20 mL) under stirring. The pH of the solution was adjusted to 7.5 using HCl (6 $mol\cdot L^{-1}$). After 20 min stirring, $EuCl_3$ (0.25 g, 0.97 mmol), $HoCl_3$ (0.25 g, 0.92 mmol), $ErCl_3$ (0.25 g, 0.91 mmol), or $TbCl_3$ (0.25 g, 0.94 mmol) was added to the solution. After another 30 min continuous stirring, the resulting solution was kept at 90 °C in a water bath for 2 h and then cooled to room temperature and filtered. Slow evaporation at room temperature resulted in colorless quadrangular prism crystals for **2-Eu**, light yellow quadrangular prism crystals for **2-Ho**, pink quadrangular prism crystals for **2-Er**, and colorless quadrangular prism crystals for **2-Er** after about 1 week, which were filtered off and air-dried. Yield: 0.59 g (33%) for **2-Eu**, 0.67 g (39%) for **2-Ho**, 0.73 g (43%) for **2-Er**, and 0.63 g (36%) for **2-Tb** based on $LnCl_3$. Elemental analysis (%) calcd for **2-Eu**: H, 1.64; C, 1.30; K, 2.12; Na, 4.97; Eu, 8.22; W, 49.73. Found: H, 1.67; C, 1.34; K, 2.00; Na, 5.13; Eu, 8.41; W, 49.59. Elemental analysis (%) calcd for **2-Ho**: H, 1.62; C, 1.29; K, 2.10; Na, 4.94; Ho, 8.86; W, 49.38. Found: H, 1.51; C, 1.36; K, 2.24; Na, 4.78; Ho, 8.75; W, 49.50. Elemental analysis (%) calcd for **2-Er**: H, 1.62; C, 1.29; K, 2.10; Na, 4.93; Er, 8.97; W, 49.32. Found: H, 1.47; C, 1.32; K, 2.27; Na, 5.10; Er, 8.74; W, 49.18. Elemental analysis (%) calcd for **2-Tb**: H, 1.63; C, 1.29; K, 2.11; Na, 4.96; Tb, 8.57; W, 49.54. Found: H, 1.58; C, 1.38; K, 2.19; Na, 5.16; Tb, 8.68; W, 49.71. IR (KBr, cm^{-1}): 3446s, 1655s, 1436w, 1378w, 1320m, 941s, 829s, 788s, 677s, 583w, 539m, 489w, 427w for **2-Eu**;

Table 1. Crystallographic Data and Structure Refinements for 1 and 2

	1-Eu	1-Ho	1-Er	1-Tb	2-Eu	2-Ho	2-Er	2-Tb
empirical formula	$C_4H_{82}Eu_4Na_{10}O_{80}W_8$	$C_4H_{82}Ho_4Na_{10}O_{80}W_8$	$C_4H_{82}Er_4Na_{10}O_{80}W_8$	$C_4H_{82}Tb_4Na_{10}O_{80}W_8$	$C_8H_{120}Eu_4K_4Na_{16}O_{148}W_{20}$	$C_8H_{120}Ho_4K_4Na_{16}O_{148}W_{20}$	$C_8H_{120}Er_4K_4Na_{16}O_{148}W_{20}$	$C_8H_{120}Tb_4K_4Na_{16}O_{148}W_{20}$
fw	3719.24	3771.12	3780.44	3747.08	7394.12	7446.00	7455.32	7421.96
cryst syst	monoclinic	monoclinic	monoclinic	monoclinic	triclinic	triclinic	triclinic	triclinic
space group	$C2/m$	$C2/m$	$C2/m$	$C2/m$	$P\bar{1}$	$P\bar{1}$	$P\bar{1}$	$P\bar{1}$
a, Å	11.9450(16)	11.8885(9)	11.9139(5)	11.9039(10)	9.9166(5)	9.9269(14)	9.898(3)	10.015(7)
b, Å	35.741(5)	35.367(3)	35.3632(17)	35.504(3)	19.4656(10)	19.319(3)	19.218(5)	19.598(13)
c, Å	9.9283(14)	9.8398(7)	9.8539(5)	9.8808(9)	19.4690(10)	19.350(3)	19.257(5)	19.640(14)
α, deg	90	90	90	90	106.2040(10)	106.232(2)	106.250(4)	106.185(10)
β, deg	109.203(2)	109.1940(10)	109.1720(10)	109.2180(10)	93.0640(10)	92.914(3)	92.812(5)	92.996(11)
γ, deg	90	90	90	90	95.3570(10)	95.152(2)	95.174(4)	95.207(11)
V, Å^{-3}	4002.8(10)	3907.3(5)	3921.3(3)	3943.3(6)	3580.6(3)	3537.4(9)	3491.8	3675(4)
Z	2	2	2	2	1	1	1	1
μ, mm^{-1}	14.703	15.901	16.089	15.330	18.003	18.687	19.069	17.760
$F(000)$	3400	3432	3440	3416	3336	3352	3356	3344
T, K	296(2)	296(2)	296(2)	296(2)	296(2)	296(2)	296(2)	296(2)
limiting indices	$-6 \le h \le 14$ $-42 \le k \le 42$ $-11 \le l \le 11$	$-8 \le h \le 14$ $-42 \le k \le 40$ $-11 \le l \le 11$	$-14 \le h \le 8$ $-42 \le k \le 41$ $-10 \le l \le 11$	$-14 \le h \le 14$ $-36 \le k \le 42$ $-11 \le l \le 11$	$-11 \le h \le 11$ $-13 \le k \le 23$ $-23 \le l \le 23$	$-11 \le h \le 11$ $-22 \le k \le 22$ $-22 \le l \le 22$	$-9 \le h \le 11$ $-22 \le k \le 21$ $-18 \le l \le 22$	$-11 \le h \le 11$ $-18 \le k \le 23$ $-23 \le l \le 23$
no. reflns collected	9890	9699	9860	9485	18430	17968	17308	18363
no. indep reflns	3490	3403	3413	3428	12490	12329	12023	12601
R_{int}	0.0506	0.0322	0.0330	0.0446	0.0279	0.0363	0.0402	0.0641
data/restrains/params	3490/8/217	3403/20/231	3413/19/230	3428/18/227	12490/12/867	12329/0/867	12023/60/867	12601/60/856
GOF on F^2	1.100	1.093	1.082	1.066	1.054	1.054	1.030	1.009
final R indices $[I > 2\sigma(I)]$	$R_1 = 0.0533$ $wR_2 = 0.1538$	$R_1 = 0.0388$ $wR_2 = 0.1075$	$R_1 = 0.0368$ $wR_2 = 0.1073$	$R_1 = 0.0518$ $wR_2 = 0.1386$	$R_1 = 0.0402$ $wR_2 = 0.0976$	$R_1 = 0.0471$ $wR_2 = 0.1184$	$R_1 = 0.0485$ $wR_2 = 0.1381$	$R_1 = 0.0612$ $wR_2 = 0.1482$
R indices (all data)	$R_1 = 0.0637$ $wR_2 = 0.1619$	$R_1 = 0.0420$ $wR_2 = 0.1097$	$R_1 = 0.0400$ $wR_2 = 0.1098$	$R_1 = 0.0561$ $wR_2 = 0.1419$	$R_1 = 0.0566$ $wR_2 = 0.1039$	$R_1 = 0.0652$ $wR_2 = 0.1256$	$R_1 = 0.0677$ $wR_2 = 0.1514$	$R_1 = 0.0891$ $wR_2 = 0.1615$

3446s, 1668s, 1440w, 1373w, 1324m, 942s, 842s, 784s, 677s, 583w, 543m, 489w, 431w for **1-Ho**; 3442s, 1664s, 1445w, 1378w, 1320m, 940s, 842s, 789s, 681s, 583w, 543w, 489w, 435w for **1-Er**; 3440s, 1666s, 1453w, 1376w, 1324m, 945s, 842s, 793s, 677s, 585w, 547w, 489w, 431w for **1-Tb**.

X-ray Crystallography. Diffraction intensity data of **1** and **2** were collected on a Bruker Apex II diffractometer equipped with a CCD bidimensional detector with the graphite-monochromated Mo Kα radiation (λ = 0.71073 Å) at 296 K. The absorption correction was based on multiple and symmetry-equivalent reflections in the data set using the SADABS program.[6a] Direct methods were used to solve their structures and locate the heavy atoms using the SHELXTL-97 program package.[6b,c] The remaining atoms were found from successive full-matrix least-squares refinements on F^2 and Fourier syntheses. No hydrogen atoms associated with water molecules were located from the difference Fourier map. All non-hydrogen atoms were refined anisotropically except for some oxygen and carbon atoms and water molecules. In order to decrease the value of the largest difference peaks in the refinements, we have to split the Eu, Ho, Er, and Tb atoms in **1** to two sites with occupancy of 50% for each site. In addition, we chose good quality single crystals of **1-Ho** and **1-Er** and again collected their intensity data at 130 K; however, we did not observe apparent improvement of the quality of diffraction data after the refinements, and the Ho and Er atoms still split to two sites. In the refinements, six Na^+ ions and 26 lattice water molecules per molecule of **1** were found from the Fourier maps. However, there are still solvent accessible voids in the check cif reports of crystal structures, suggesting that some counter cations and water molecules should exist in the structures that cannot be found from the weak residual electron peaks. These counter cations and water molecules are highly disordered and attempts to locate and refine them were unsuccessful. The SQUEEZE program was used to remove scattering from the highly disordered cations and molecules, and new .HKL files were generated. The structures were solved using the newly generated .HKL files. On the basis of charge-balance considerations, elemental analyses, and TG analyses, another four Na^+ ions and four water molecules were directly added to each molecular formula. Crystallographic data and structure refinements for **1** and **2** are summarized in Table 1. Crystallographic data for this paper have been deposited in the Cambridge Crystallographic Data Centre with CCDC 995656−995661 and 1007747−1007748 for **1-Eu**, **1-Ho**, **1-Er**, **2-Eu**, **2-Ho**, **2-Er**, **1-Tb**, and **2-Tb**, respectively.

RESULTS AND DISCUSSION

Structure Description. Both **1** and **2** were prepared by means of $Na_2WO_4{\cdot}2H_2O$, oxalic acid, and $LnCl_3$ in the presence of alkaline cations. During the course of the synthetic exploration, several key points should be mentioned here: (1) The nature of Ln cations strongly influences the structural type of products. When the early Ln cations (La^{3+}−Sm^{3+}) were used in this system, we obtained Peacock and Weakley's $[Ln(W_5O_{18})_2]^{n-}$ analogues.[7a] Accordingly, when the late Ln cations (Eu^{3+}−Lu^{3+}) were utilized, oxalate-connective Ln-substituted isopolyoxotungstates **1** and **2** were made. (2) The pH value plays a very important role in the formation of **1** and **2**. Experimental results prove that **1** and **2** can be separated when the pH values are in the range of 6.5−7.8, and when the pH value is at 7.5, their yields are the highest. The pH value being higher than 7.8 will lead to the formation of amorphous precipitates, while the pH value being lower than 6.5 will form paradodecatungstate derivatives. (3) The introduction of KCl to the synthetic conditions of **1** gave rise to the isolation of **2**. The detailed formation mechanisms were not well understood. We speculate that the size of alkaline cations may be the main reason that leads to the structural difference of **1** and **2**. Such phenomenon has been previously encountered.[7b] For example, Gutiérrez-Zorrilla et al. found that the structures of the outcomes highly depend on the types of alkaline cations. When Rb^+, K^+, or Na^+ acetate buffers, respectively, are used, three different silicotungstates, $Rb_7[Cu_2(ac)_2(phen)_2(H_2O)_2][Cu_3(ac)_3(phen)_3(H_2O)_3]$ $[Si_2W_{22}Cu_2O_{78}(H_2O)]{\cdot}18H_2O$, $K_4[\{SiW_{11}O_{39}Cu(H_2O)\}\{Cu_2(ac)_2\ (phen)_2(H_2O)\}]{\cdot}14H_2O$, and $K_8[\{Si_2W_{22}Cu_2O_{78}(H_2O)\}\{Cu_2(ac)_2\ (phen)_2(H_2O)\}_2]{\cdot}40H_2O$ (phen =1,10-phenanthroline, ac = acetate) were respectively obtained.[7b]

X-ray single-crystal diffraction indicates that **1** crystallizes in the monoclinic space group $C2/m$ and forms a double-oxalate-bridging di-Ln substituted Lindqvist-type dimer with a rectangular tetra-Ln cluster, whereas **2** belongs to the triclinic space group $P\bar{1}$ and forms a single-oxalate-connective mono-Ln^{III} Lindqvist-type tetramer with a square tetra-Ln cluster. Herein, we take **1-Eu** and **2-Eu** as examples to discuss their structures. The skeleton structure of **1-Eu** consists of a centrosymmetric dimer $[Eu_2(C_2O_4)(H_2O)_4(OH)W_4O_{16}]_2^{10-}$ (Figure 1a; Figure S1, Supporting Information) that can be viewed as a combination of two di-Eu^{III} substituted Lindqvist segments via two oxalate linkers. The divacant Lindqvist segment $[W_4O_{16}]^{8-}$ is derived from the parent $[W_6O_{19}]^{2-}$ polyoxoanion by removal of two edge-sharing WO_6 octahedra, which is completely different from the planar $[W_4O_{16}]^{8-}$ (Figure S2, Supporting Information) unit observed in $\{[(\alpha\text{-}AsW_6O_{26})Ni_6(OH)_2(H_2O)_3(en)(B\text{-}\alpha\text{-}AsW_9O_{34})]_2[W_4O_{16}][Ni_3(H_2O)_2(en)]_2\}^{16-}$.[7c] Two Eu^{III} ions are simultaneously incorporated to a divacant $[W_4O_{16}]^{8-}$ fragment by one μ_6-O and five μ_2-O atoms (Figure 1b). Furthermore, two Eu^{III} ions are further combined together via sharing a μ_6-O and a μ_2-OH generating a di-Eu^{III} cluster. As far as we know, such a di-Ln substituted Lindqvist fragment is observed for the first time. The most remarkable feature in **1-Eu** is that two Eu^{III} clusters are linked together through two tetradentate oxalates giving rise to a rectangular tetra-Eu^{III} cluster (Figure 1c), which is first discovered in POM chemistry, albeit oxalate-bridging mono-RE substituted Keggin phosphotungstates $\{[(\alpha\text{-}PW_{11}O_{39})RE(H_2O)]_2(C_2O_4)\}^{10-}$ (RE = Y^{III}, Dy^{III}, Ho^{III}, or Er^{III}) (**3**) and oxalate-bridging di-Tm substituted Keggin species $\{(\alpha\text{-}x\text{-}PW_{10}O_{38})Tm_2(C_2O_4)(H_2O)_2\}^{3-}$ (**4**) have been already reported.[7d] The biggest differences between **1** and **3** or **4** lie in two aspects: (a) **1** contains di-Ln substituted Lindqvist isopolyoxotungstate segments; in contrast, **3** and **4**, respec-

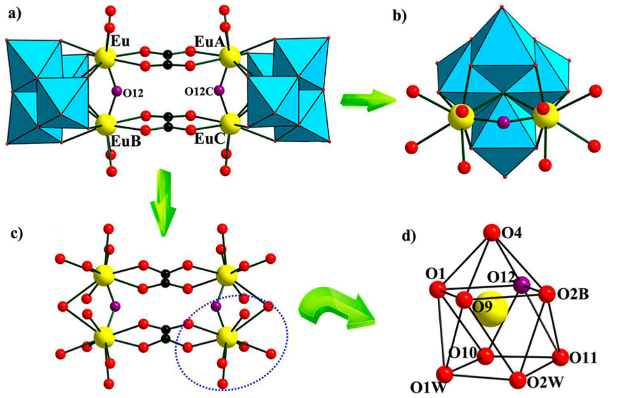

Figure 1. (a) Dimeric structure in **1-Eu**, (b) incorporation of the di-Eu^{III} cluster to the divacant Lindqvist fragment, (c) rectangular tetra-Eu^{III} cluster, and (d) monocapped square antiprism geometry of the Eu^{III} cation. The atoms with "'A−C"' in their labels are symmetrically generated (A, *x*, −*y*, *z*; B, −*x*, *y*, 1 − *z*; C, −*x*, −*y*, 1 − *z*). Na^+ cations and lattice water molecules are omitted for clarity.

tively, include mono-RE and di-Tm substituted Keggin heteropolyoxotungstate fragments; (b) two di-Ln substituted Lindqvist subunits in **1** are connected to each other by two oxalates, while two lacunary Keggin fragments are combined together via one oxalate. Additionally, two vacant sites of the Lindqvist unit in **1** are situated in the adjacent position, whereas two defect sites of the Keggin unit in **4** are in the opposite direction. The crystallographically independent Eu^{3+} cation resides in the nine-coordinate monocapped square antiprism where three μ_2-O atoms from a $[W_4O_{16}]^{8-}$ segment, a hydroxyl group, two carboxylic O atoms of an oxalate ligand, and two water ligands define two bottom surfaces of the square antiprism and one μ_6-O atom from the $[W_4O_{16}]^{8-}$ segment is situated on the capped site (Figure 1d). In addition, it should be pointed out that there are two crystallographically unique Na^+ ($Na1^+$ and $Na2^+$) cations in **1-Eu**, and two adjacent octahedral $Na1^+$ cations are combined together to create dinuclear $[Na_2O_2(H_2O)_8]^{2-}$ clusters, which are further bridged by square pyramid $Na2^+$ cations producing the well-structured sinusoidal chain (Figure 2). More intriguingly, dimeric $[Eu_2(C_2O_4)(H_2O)_4(OH)W_4O_{16}]_2^{10-}$ structural moieties are joined together by these sinusoidal chains propagating the extraordinary 3-D pillar-supporting architecture (Figure 3; Figure S3, Supporting Information), in which $[Eu_2(C_2O_4)(H_2O)_4(OH)W_4O_{16}]_2^{10-}$ structural moieties serve as the pillars between sinusoidal chains and interspaces are filled with a large number of lattice water molecules.

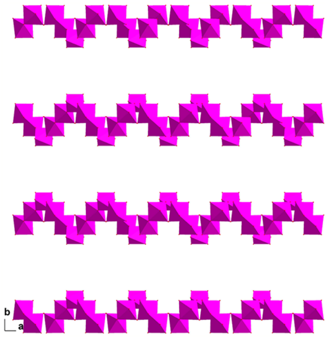

Figure 2. Polyhedral view of the well-structured sinusoidal chains built by dinuclear $[Na1_2O_2(H_2O)_8]^{2-}$ clusters through square pyramid $Na2^+$ linkers in **1-Eu**.

Different from **1-Eu**, the backbone of **2-Eu** is composed of four mono-Eu^{III} substituted Lindqvist segments with four oxalate connectors (Figure 4a; Figure S4, Supporting Information), in which the monovacant Lindqvist $[W_5O_{18}]^{6-}$ subunit originates from the removal of a W═O group from the $[W_6O_{19}]^{2-}$ matrix. Such a monovacant Lindqvist subunit has been previously documented.[8] The presence of two crystallographically unique Eu^{3+} ions ($Eu1^{3+}$ and $Eu2^{3+}$) makes the tetrameric $[Eu(C_2O_4)W_5O_{18}]_4^{20-}$ unit lose D_{4h} symmetry and has centric symmetry. Each Eu^{3+} ion is anchored in the monovacant position of the $[W_5O_{18}]^{6-}$ matrix via one μ_6-O and four μ_2-O atoms (Figure 4b). The most striking structural characteristic of **2-Eu** is that four Eu^{3+} ions are concatenated by virtue of four oxalate anions generating an unseen square tetra-Eu^{III} cluster in POM chemistry (Figure 4c), which is distinct from linear three-oxalate-bridging tetra-Yb^{III} clusters in $[\{Yb(POM)\}_4(C_2O_4)_3(H_2O)_4]^{n-}$ (POM = α-$SiW_{11}O_{39}$, n = 26; α_2-$P_2W_{17}O_{61}$, n = 34).[9] Two crystallographically unique Eu^{3+} cations in **2-Eu** also adopt the nine-coordinate monocapped square antiprism geometry, in which four μ_2-O atoms from a $[W_5O_{18}]^{6-}$ subunit and four carboxylic O atoms from two oxalates constitue two bottom surfaces of the square antiprism and one μ_6-O atom from the $[W_5O_{18}]^{6-}$ subunit occupies the capped site (Figure 4d). In addition, the alignment of tetrameric $[Eu(C_2O_4)W_5O_{18}]_4^{20-}$ units across the *bc* plane is shown in Figure 5. As far as we know, **2** still is the first organic–inorganic hybrid square Ln-substituted POM though two inorganic square TM substituted heteropolyoxotungstates; $[\{\beta$-$Ti_2SiW_{10}O_{39}\}_4]^{24-}$ and $[(\alpha$-$PW_{10}Fe_2\ O_{39})_4]^{26-}$ have been addressed by Kortz and Dolbecq.[10]

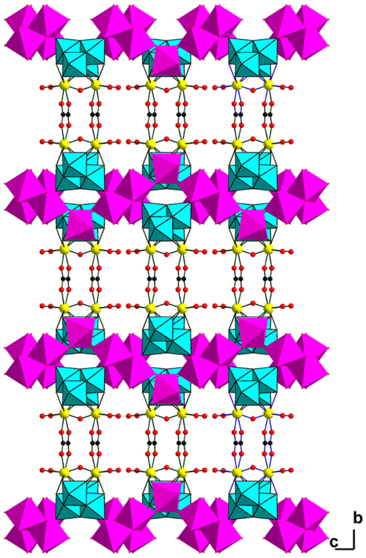

Figure 3. View of the extraordinary 3-D pillar-supporting architecture along the *a* axis in **1-Eu**. Lattice water molecules are omitted for clarity.

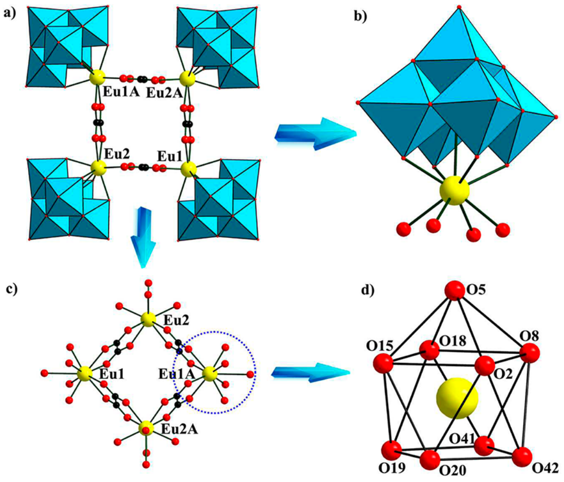

Figure 4. (a) Tetrameric structure in **2-Eu**, (b) incorporation of a Eu^{III} ion to the monovacant Lindqvist fragment, (c) square tetra-Eu^{III} cluster, and (d) square antiprism geometry of the Eu^{III} cation. Na^+ and K+ cations and lattice water molecules are omitted for clarity.

Thermal Properties. To investigate the thermal stability and determine the number of lattice water molecules of **1** and **2**, TG analyses of **1-Eu**, **1-Ho**, **1-Er**, **2-Eu**, **2-Ho**, and **2-Er** have been conducted on crystalline samples under N_2 atmosphere with a heating rate of 10 °C/min in the temperature range of 25–700 °C (Figures S5 and S6, Supporting Information). All the TG curves exhibit two-step weight loss. The first-step

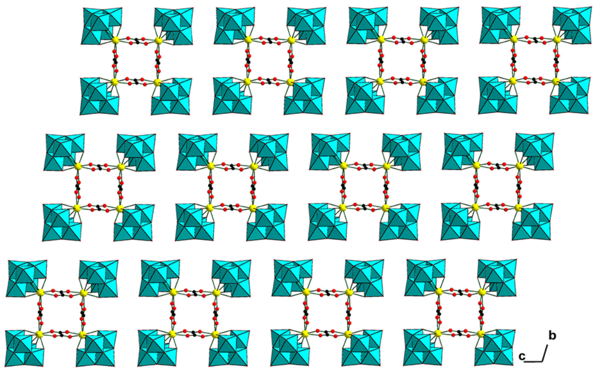

Figure 5. Packing view of **2-Eu** along the *a* axis. Na^+ and K+ cations and lattice water molecules are omitted for clarity.

gradual weight loss of 17.80% for **1-Eu**, 17.63% for **1-Ho**, and 18.53% for **1-Er** occurs between 25 and 365 °C, which corresponds approximately to the liberation of 30 lattice water molecules and eight coordination water molecules (calcd 18.41% for **1-Eu**, 18.15% for **1-Ho**, 18.12% for **1-Er**). The second-step weight loss from 365 to 700 °C of 4.98% for **1-Eu**, 4.70% for **1-Ho**, and 6.01% for **1-Er** is approximately assigned to the dehydration of two hydroxylic groups and the removal of two $C_2O_4^{2-}$ ligands (calcd 5.22% for **1-Eu**, 5.15% for **1-Ho**, 5.13% for **1-Er**). Correspondingly, the first weight loss of 15.30% for **2-Eu**, 14.41% for **2-Ho**, and 14.00% for **2-Er** occurs between 25 and 180 °C, which corresponds approximately to the liberation of 60 lattice water molecules (calcd 14.62% for **2-Eu**, 14.52% for **2-Ho**, 14.50% for **2-Er**). The second-step weight loss from 180 to 700 °C of 4.88% for **2-Eu**, 4.87% for **2-Ho**, and 4.97% for **2-Er** is approximately assigned to the dehydration of two hydroxylic groups and the removal of two $C_2O_4^{2-}$ ligands (calcd 4.76% for **2-Eu**, 4.73% for **2-Ho**, 4.72% for **2-Er**).

IR Spectra. IR data of the as-synthesized samples **1** and **2** have been recorded on a Nicolet 170 SXFT−IR spectrometer using KBr pellets in the range of 4000−400 cm^{-1} (Figures S7 and S8, Supporting Information). The existence of the polyoxotungstate clusters and oxalate ligands in the crystalline solids **1** and **2** are elucidated by their IR spectra in the solid state. In the region of 1000−650 cm^{-1}, IR spectra of **1** and **2** display the characteristic vibration patterns derived from the W−O skeleton.[11] The strong absorption peak centered at 942−940 cm^{-1} in **1** and **2** is ascribed to the $\nu(W{=}O)$ stretching vibration. Two groups of vibration signals appearing at 842−677 cm^{-1} in **1** and **2** are assigned to the $\nu(W{-}O{-}W)$ stretching vibration. In the high-frequency region, the spectra of **1** and **2** are dominated by an intense and wide absorption peak centered at 3432−3446 cm^{-1}, which arises from the $\nu(O{-}H)$ stretching mode of the water molecules,[12] while in the lower-frequency region, an intense band centered at 1655−1668 cm^{-1} results from the $\nu(OH)$ bending vibration of the water molecules. It should be noted that the asymmetric stretching vibration band of the carboxylate group of oxalate ligands overlaps the $\nu(O{-}H)$ bending vibration band of lattice water molecules. In general, the carboxylic group is expected to give rather intense bands from asymmetric and symmetric stretching vibration in the fingerprint region of the IR spectrum.[12a,13] As a result, the strong absorption band at 1668−1655 cm^{-1} can be assigned to the asymmetric stretching vibration of the carboxylic group [denoted as $\nu_{as}(CO_2^-)$], while the absorption band at 1324−1320 cm^{-1} corresponds to the symmetric stretching vibration of the carboxylic group [denoted as $\nu_s(CO_2^-)$]. In comparison with the free oxalate ligand (the asymmetric and symmetric stretching vibrations are observed at 1690 and 1350 cm^{-1}),[14] the $\nu_{as}(CO_2^-)$ and $\nu_s(CO_2^-)$ vibration bands for **1** and **2** have obvious red-shifts of 22−35 and 26−30 cm^{-1}, respectively, indicating that the oxalate ligands coordinate to the Ln^{III} cations. Generally, the difference ($\Delta\nu$) between $\nu_{as}(CO_2^-)$ and $\nu_s(CO_2^-)$ in the IR spectrum has been successfully used to derive information regarding bonding modes of the carboxylic group.[15] The $\Delta\nu$ of 335−344 cm^{-1} suggests the bridging coordination mode of the carboxylic groups in **1** and **2**. The weak vibration bands between 1445 and 1320 cm^{-1} can be attributed to the $\nu(C{-}O)$ bending vibration of the oxalate ligands. A close inspection of the IR spectra of **1** and **2** can reveal that the $\nu(C{-}O)$ bending vibration bands in **2** are more complicated than those in **1**, which is mainly because there are two crystallographically independent oxalate ligands in the structures of **2**, whereas there is only one crystallographically independent oxalate ligand in the structures of **1**. In addition, there was no appearance of the Ln−O stretching vibration in the IR region probably due to predominant ionic interactions between vacant isopolyoxotungstate units and Ln^{III} cations.[16]

Photoluminescence Studies. The luminescent behavior of Ln-based compounds has attracted increasing interest due to the high color purity and technological applications in light-emitting diodes, lasers, plasma displays, and sensory probes and optical amplifiers, etc.[17] Because the good shielding of the 4f electrons by the outer 5s and 5p electrons leads to well-defined absorption and emission bands,[18] Ln ions still keep their atomic properties upon complex formation. Generally speaking, the f−f transitions are spin- and parity-forbidden; therefore, the luminescence of Ln-based compounds is normally generated through the "antenna effect".[19] It has been proven that the Ln-centered photoluminescence emission can be sensitized by either energy transfer from ligand-to-metal charge-transfer (LMCT) excited states centered on POMs[5a,b] or organic chromophores containing the electron-conjugate system,[5c,d] which can effectively absorb light and transfer excitation energy to Ln centers. As a result, the photoluminescence properties of **1-Eu**, **1-Tb**, **2-Eu**, and **2-Tb** in the solid-state have been measured at room temperature (Figure 6). Excitation of the as-synthesized solids at 394 nm exhibits five groups of characteristic emission bands at 580 nm; 591, 594 nm; 615, 618, 621 nm; 652 nm; and 691,701 nm for **1-Eu** (Figure 6a) and at 580 nm; 591, 593, 596 nm; 615, 618, 622 nm; 652 nm; 690, 693, and 701 nm for **2-Eu** (Figure 6b), which are respectively attributed to $^5D_1 \rightarrow {}^7F_2$, $^5D_0 \rightarrow {}^7F_1$, $^5D_0 \rightarrow {}^7F_2$, $^5D_0 \rightarrow {}^7F_3$, and $^5D_0 \rightarrow {}^7F_4$ transitions of Eu^{III} ions.[20a] In general, the intensity of the magnetic dipole $^5D_0 \rightarrow {}^7F_1$ transition hardly varies with the crystal field strength acting on Eu^{III} ions whereas the electric dipole $^5D_0 \rightarrow {}^7F_2$ transition is hypersensitive to the chemical bonds in the vicinity of Eu^{III} ions. The $^5D_0 \rightarrow {}^7F_1$ transition is dominant in a centrosymmetric environment, while the $^5D_0 \rightarrow {}^7F_2$ transition becomes the strongest in a noncentrosymmetric situation.[20b,c] The intensity of the $^5D_0 \rightarrow {}^7F_2$ transition increases as the site symmetry of Eu^{III} ions decreases. As a result, the intensity ratio of $^5D_0 \rightarrow {}^7F_2/{}^5D_0 \rightarrow {}^7F_1$ often functions as a criteria for the site symmetry of the Eu^{III} cations.[20d] The intensity ratios in **1-Eu** and **2-Eu** are 5.2 and 5.4, reflecting the low site symmetry of the Eu^{III} ions, which is consistent with the distorted

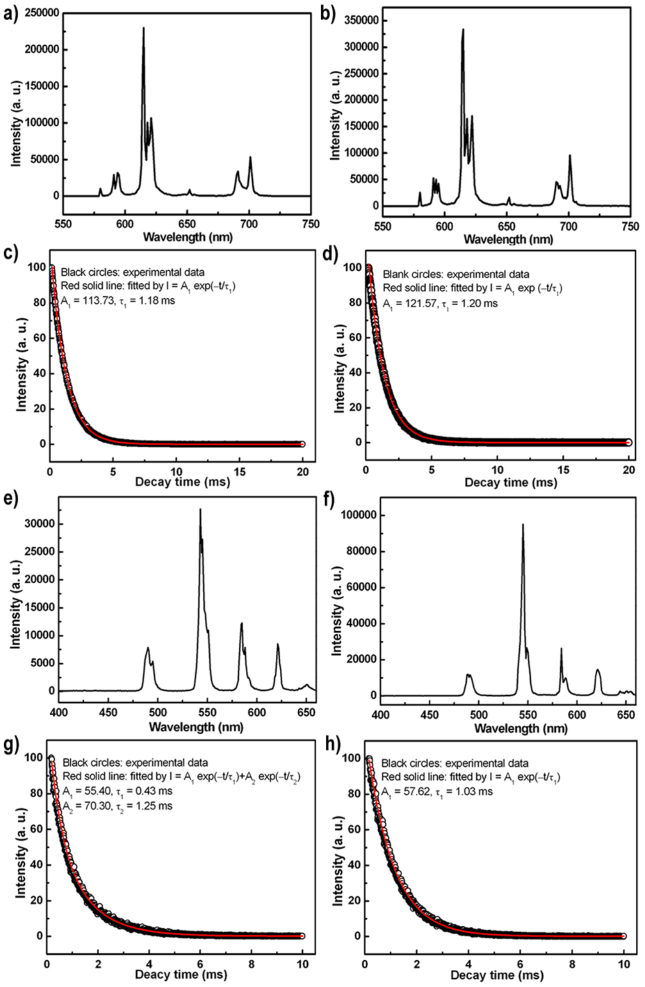

Figure 6. (a, b) Photoluminescence emission spectra of **1-Eu** and **2-Eu**, (c, d) luminescence decay curves of **1-Eu** and **2-Eu**, (e, f) photoluminescence emission spectra of **1-Tb** and **2-Tb**, and (g, h) luminescence decay curves of **1-Tb** and **2-Tb**.

monocapped square antiprism geometry of Eu^{III} cations. By monitoring the emission of the Eu^{III} $^5D_0 \rightarrow {}^7F_2$ transition at 615 nm, we have also obtaine the excitation spectra of **1-Eu** and **2-Eu** (Figures S9 and S10, Supporting Information). In the excitation spectra of **1-Eu** and **2-Eu,** the broad band between 250 and 350 nm is attributed to the absorption of $[W_4O_{16}]^{8-}$ or $[W_5O_{18}]^{6-}$ segments that can sensitize subsequent Eu-centered emission, which coincides with the conclusion made by Yamase that photoexcitation of the O → M (M = W, Mo, or Nb) LMCT bands of polyoxometalloeuropates sensitizes an Eu^{III} emission with a single exponential decay.[5a] Moreover, the emission spectrum of solid-state oxalic acid upon excitation at 394 nm has been also measured (Figure S11, Supporting Information), in which an emission band at 611 nm is observed, indicating that oxalate ligands to some extent contribute to the photoluminescence of **1-Eu** and **2-Eu**. Notably, the emission intensity of **1-Eu** is somewhat lower than that of **2-Eu** although the percentage of Eu^{III} ingredients in **1-Eu** is higher than that in **2-Eu**, the major reason for which may have two factors: (a) coordination waters and OH groups in **1-Eu** partly quench emission and shorten luminescence lifetime through nonradiative relaxation processes;[21a] (b) in **2-Eu**, each Eu^{III} cation is coordinated by a $[W_5O_{18}]^{6-}$ subunit and two $C_2O_4^{\ 2-}$ ligands that more effectively sensitize the Eu^{III} emission than those in **1-Eu**. This phenomenon has been observed in **1-Tb** and **2-Tb** (*vide infra*). The decay curves of **1-Eu** and **2-Eu** can be well fitted to a single exponential function as $I = A\ \exp(-t/\tau)$, (where τ is the $1/e$ lifetime of the Ln ion) ,and the fitting parameters are shown in Figure 6c,d. The fluorescence lifetimes are 1.18 and 1.20 ms, respectively. Additionally, the luminescence photographs of **1-Eu** and **2-Eu** under irradiation of a 254 nm UV lamp are shown in Figure S12 in Supporting Information.

The solid-state photoluminescence spectra of **1-Tb** and **2-Tb** upon excitation at 369 nm are displayed in Figure 6e,f, respectively. Both emission spectra exhibit four groups of bands at 490, 495 nm; 543, 545 nm; 584, 588 nm; and 621 nm for **1-Tb**, and 488, 490 nm; 545, 550 nm; 584, 589 nm; and 621 nm for **2-Tb**, which are assigned to the $^5D_4 \rightarrow {}^7F_6$, $^5D_4 \rightarrow {}^7F_5$, $^5D_4 \rightarrow {}^7F_4$, and $^5D_4 \rightarrow {}^7F_3$ transitions, respectively, of Tb^{III} cations.[5c,21b,c] By monitoring Tb^{III} $^5D_4 \rightarrow {}^7F_5$ emission at 543 nm, both excitation spectra have also been collected (Figures S13 and S14, Supporting Information). Obviously, a broad band between 250 and 350 nm attributable to the absorption of $[W_4O_{16}]^{8-}$ or $[W_5O_{18}]^{6-}$ segment is seen in their excitation spectra, which suggests that the photoluminescence emissions of **1-Tb** and **2-Tb** are from POM-centered LMCT processes, which are somewhat distinct from the case encountered by Boscovic et al. in $[Tb_8(pic)_6(H_2O)_{22}(B\text{-}\beta\text{-}AsW_8O_{30})_4(WO_2(pic))_6]^{12-}$[5c] and the conclusion made by Yamase that room-temperature sensitization by the POM-centered LMCT path is not efficient for the Tb^{III} cations because of radiationless deactivation involving Tb^{IV}–W^{V} charge-transfer states.[5a] The green luminescence photographs of **1-Tb** and **2-Tb** under the irradiation of a 254 nm UV lamp are shown in Figure S15 in Supporting Information. For **1-Tb**, its decay behavior can be fitted to a biexponential function as $I = A_1\ \exp(-t/\tau_1) + A_2\ \exp(-t/\tau_2)$, affording lifetimes of $\tau_1 = 0.43$ ms and $\tau_2 = 1.25$ ms (Figure 6g). This behavior is similar to that of the hydrated Tb^{III} complexes,[5c,d,21d] which is in accordance with the fact that each Tb^{III} cation is coordinated by two water ligands based on the single-crystal structural analysis of **1-Tb**. In contrast, the decay behavior of **2-Tb** can be fitted to single exponential function with the lifetime of 1.03 ms (Figure 6h). This decay behavior is similar to Tb^{III} complexes without water ligands.[21e]

Magnetic Properties. Currently, Ln chemistry is a worldwide topical research area and has attracted increasing interest due to its fascinating physicochemical properties and various applications as functional materials.[22] Ln cations with large spin moments may be a good option for designing molecular magnetic materials; however, the magnetic exchange constants in most cases are small, the main reason for which is that the 4f orbitals are very efficiently shielded by fully occupied 5s and 5p orbitals, leading to less involvement in bonds between neighboring Ln centers.[23] To date, the nature and magnitude of exchange interactions within Ln centers (except for diamagnetic La^{III}, Lu^{III}, and spin-only Gd^{III}) and the magnetic evolution along the Ln series is much less known, principally because the orbital contribution and crystal-field effects generally play an extremely important role in the magnetism of most Ln compounds, which makes the quantitative analyses of magnetism become rather intricate.[23a,24] Usually, the large spin–orbital coupling and interelectronic repulsion partly removes the degeneracy of the ^{2S+1}L group term of Ln cations, leading to the $4f^n$ configuration (^{2S+1}L group term) splitting into $^{2S+1}L_J$ spectroscopic states. Each state further splits into Stark components by the crystal-field perturbation.[23a,24a] The number of Stark components is related to the symmetry site of the Ln cation.[25] Because of smaller crystal-field effects and the larger spin−orbit orbital coupling for f electrons compared with the d electrons of transition-metal ions, the orbital angular momentum for Ln cations is more crucial than that for transition-metal cations.[26] Therefore, it would be difficult to analyze magnetic properties of Ln compounds in that Ln cations (Ln ≠ La^{III}, Gd^{III}, or Lu^{III}) have the first-order angular momentum that prevents using the spin-only isotropic Hamiltonian.[27a−c] At room temperature, all the Stark sublevels arising from the ground state are populated. Upon cooling, a progressive depopulation of these sublevels occurs. Even for mononuclear Ln compounds, the temperature variation can result in the magnetic susceptibility deviating from the Curie law.[25] In polynuclear compounds, the thermal variation of magnetic susceptibilities relies on the population of Stark levels of Ln cations and magnetic couplings within Ln centers. Thus, the $\chi_M T$ values of most of Ln compounds at room temperature are near the calculated values making use of the free-ion approximation that only $^{2S+1}L_J$ ground state is thermally populated and the second-order contribution is ignored.[27c−e] For Sm^{III} and Eu^{III} compounds, the magnetic susceptibility would be affected by the thermally populated excited state owing to the small energy separation between the $^{2S+1}L_J$ ground state and the first excited state.[23a] As a result, the possible thermal population of the excited states should be considered with regard to Sm^{III} and Eu^{III} compounds. For these reasons, magnetic susceptibility measurements of **1** and **2** have been carried out for polycrystalline samples at an applied field of 1 kOe in the range of 2−300 K (Figures 7 and 8). In addition, recent particular attention has been paid to utilizing Ln cations to design novel single-molecule magnets (SMMs) for the sake of their significant magnetic anisotropy arising from the large, unquenched orbital angular momentum.[28] In this respect, the Tb^{III} and Dy^{III} cations seem to be especially useful. As a result, the alternating current magnetic susceptibilities of **1-Ho**, **1-Er**, **1-Tb**, **2-Ho**, **2-Er**, and **2-Tb** have been also carried out under a zero direct current field and an oscillation of 3 Oe.

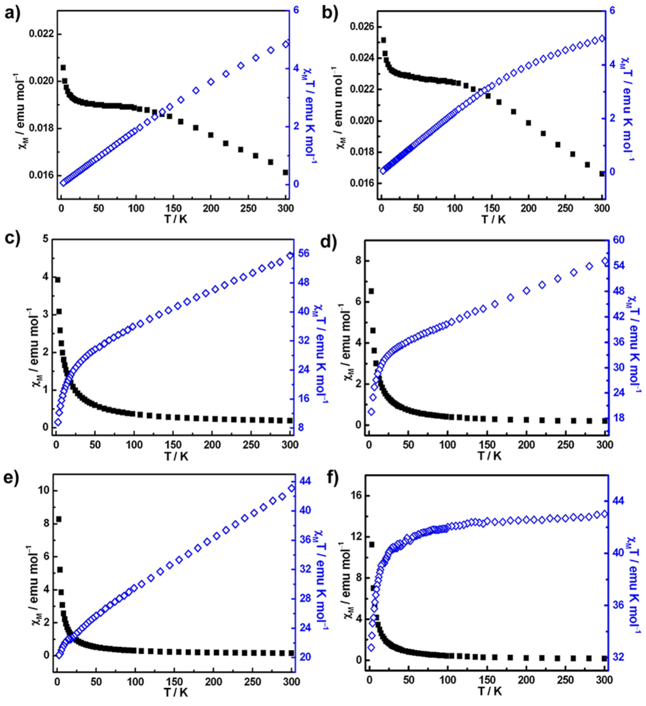

Figure 7. Temperature dependence of the magnetic susceptibility for (a) **1-Eu**, (b) **2-Eu**, (c) **1-Ho**, (d) **2-Ho**, (e) **1-Er**, and (f) **2-Er** between 2 and 300 K.

The magnetic susceptibility behaviors of **1-Eu** and **2-Eu** are very similar. χ_M slowly increases from 0.017 emu mol^{-1} at 300 K for **1-Eu** and **2-Eu** to 0.019 emu mol^{-1} for **1-Eu** and 0.023 emu mol^{-1} for **2-Eu** at 76 K, and then tends to plateau. Below 13 K, χ_M sharply rises to reach the maximum of 0.023 emu mol^{-1} for **1-Eu** and 0.026 emu mol^{-1} for **2-Eu** at 2 K (Figure 7a,b). The slight increase in the χ_M value below 13 K is owing to the unavoidable presence of a few parts per million of Ln ions with paramagnetic ground state in the samples.[27b] At 300 K, $\chi_M T$ is 4.97 emu K mol^{-1} for **1-Eu** and 4.98 emu K mol^{-1} for **2-Eu**. As temperature decreases, $\chi_M T$ continuously declines to 0.04 emu K mol^{-1} for **1-Eu** and 0.05 emu K mol^{-1} for **2-Eu** at 2 K. At 2.0 K, $\chi_M T$ is very close to 0, indicating that the nonmagnetic $J = 0$ ground state ($^7F_0$) of the Eu(III) ion is populated at 2 K[29,27b] and there is no contribution of Stark sublevel from the crystal field. Therefore, the declining of $\chi_M T$ upon cooling for **1-Eu** and for **2-Eu** prevailingly originates from the progressive depopulation of the excited state of Eu^{III} cations, which is very similar to the magnetic phenomenon observed in a reported dinuclear europium complex [$Eu_2(4\text{-cba})_6(phen)_2(H_2O)_2$].[23a] In general, the spin−orbital coupling makes the ^7F ground term of the Eu^{III} cation split into seven states ($^7F_0$, $^7F_1$, $^7F_2$, $^7F_3$, $^7F_4$, $^7F_5$, and $^7F_6$). Owing to the small energy separation between the ground state and the first excited state, the first excited state can be thermally populated at room temperature and above.[23a] As temperature descends, the progressive depopulation of excited states happens, which results in the magnetic behavior significantly deviating from the Curie−Weiss law predicted by the free-ion approximation (Figure S16a,b, Supporting Information).[30]

The magnetic behaviors for **1-Ho** and **2-Ho** are very similar (Figures 7c,d). The χ_M slowly rises from 0.19 emu mol^{-1} for **1-Ho** and 0.18 emu mol^{-1} for **2-Ho** at 300 K to 0.99 emu mol^{-1} for **1-Ho** at 25 K and 1.60 emu mol^{-1} for **2-Ho** at 20 K, and then exponentially arrives at the maximum of 4.26 emu mol^{-1} for **1-Ho** and 8.26 emu mol^{-1} for **2-Ho** at 2 K. The room temperature $\chi_M T$ value is equal to 55.53 and 55.21 emu K mol^{-1} for **1-Ho** and **2-Ho**, respectively, and is nearly consistent with the expected value (56.28 emu K mol^{-1}) for four noninteracting Ho^{III} cations ($S = 2$, $L = 6$, $^5I_8$, $J = 8$, $g = 5/4$).[26,31] Upon cooling, the $\chi_M T$ value reduces gradually to 8.47 and 16.53 emu K mol^{-1} at 2 K for **1-Ho** and **2-Ho**, respectively. The observed lowering of $\chi_M T$ suggests an antiferromagnetic coupling interaction within Ho^{III} centers, but the thermal depopulation of the Stark sublevels of the Ho^{III} cation ground states may also participate in this.[32] This conclusion can be also further confirmed by the negative Weiss constant $\theta = -129.95$ K for **1-Ho** and -109.87 K for **2-Ho** (Figure S16c,d, Supporting Information). The smaller $\chi_M T$ value at 2 K and the larger Weiss constant for **1-Ho** than those for **2-Ho** indicate that the antiferromagnetic coupling within Ho^{III} centers in **1-Ho** is larger than that in **2-Ho**, mainly because the magnetic coupling interaction within Ho^{III} centers in **1-Ho** can be collectively mediated by OH$^-$ and oxalate bridges while the magnetic interaction in **2-Ho** can be mediated only by oxalate bridges. This phenomenon is also observed in **1-Er** and **2-Er** (*vide infra*).

The plots of $\chi_M T$ and χ_M versus T for **1-Er** and **2-Er** are shown in Figure 7e,f, respectively. The $\chi_M T$ value at 300 K is

43.09 emu K mol^{-1} for **1-Er** and 43.05 emu K mol^{-1} for **2-Er**, which is slightly lower than the theoretical value of 45.92 emu K mol^{-1} expected for four independent Er^{III} ions ($S = 3/2$, $L = 6$, $^4I_{15/2}$, $g = 6/5$),[33] which can be attributed to the crystal-field splitting of the ground state ($^4I_{15/2}$) of the Er^{III} cation.[34] As temperature is lowered, the $\chi_M T$ value slowly decreases to 19.79 emu K mol^{-1} for **1-Er** and 32.75 emu K mol^{-1} for **2-Er** at 2 K. The magnetic susceptibility data of **2-Er** in the range of 300−2 K can be well described by the Curie−Weiss law with Curie constant $C = 43.03$ emu mol^{-1} K and Weiss constant $\theta = -2.01$ K (Figure S16f, Supporting Information); however, the plot of $\chi_M{}^{-1}$ versus T between 2 and 300 K for **1-Er** does not obey the Curie−Weiss law (Figure S16e, Supporting Information). Thus, it can be concluded that the decreasing of $\chi_M T$ versus T for **2-Er** mainly stems from the thermal depopulation of the Er^{III} excited states (Stark sublevels of the $^2H_{11/2}$, $^4I_{13/2}$, and $^4S_{3/2}$ states)[27c,35] whereas the magnetic character of **1-Er** should be considered a clear signature of dominating antiferromagnetic interactions as well as the thermal depopulation of the Er^{III} excited states.[34,36] The larger Weiss constant (−133.69 K) of **1-Er** derived from the fitting of Curie−Weiss law between 145 and 300 K can also support the dominating antiferromagnetic interactions with Er^{III} centers.

The thermal variation of magnetic susceptibilities of **1-Tb** and **2-Tb** are shown in Figure 8. At 300 K, the $\chi_M T$ value is 47.10 emu K mol^{-1} for **1-Tb** and 47.21 emu K mol^{-1} for **2-Tb**, which is in good agreement with the expected value (47.27 emu K mol^{-1}) for four noninteracting Tb^{III} ions ($S = 3$, $L = 3$, $J = 6$, $^7F_6$, $g = 3/2$).[37] When the temperature is lowered, the $\chi_M T$ value decreases gradually to a value of 12.28 emu K mol^{-1} for **1-Tb** and 22.77 emu K mol^{-1} for **2-Tb** at 2 K. For **1-Tb**, the plot of $\chi_M{}^{-1}$ versus T in the temperature range of 300−144 K obeys the Curie−Weiss law affording $\theta = -154.05$ K (Figure S17a, Supporting Information). For **2-Tb**, the susceptibility data well conform to the Curie−Weiss law over the whole temperature range with $\theta = -9.38$ K (Figure S17b, Supporting Information). It can be concluded that the decrease of $\chi_M T$ for **1-Tb** and for **2-Tb** is governed by the thermal depopulation of the Stark levels of the Tb(III) ion[38] and antiferromagnetic coupling interaction within Tb^{III} centers. We presume that antiferromagnetic interactions in **1-Tb** make its magnetic susceptibility deviate from the Curie−Weiss law and produce large negative θ value, while the very weak antiferromagnetic interactions in **2-Tb** may lead to adhering to the Curie−Weiss law with the small negative θ value.

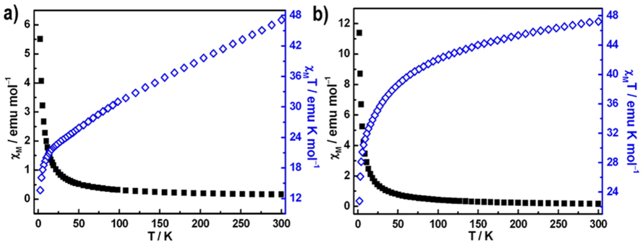

Figure 8. Temperature dependence of the magnetic susceptibility for (a) **1-Tb** and (b) **2-Tb** between 2 and 300 K.

In order to probe whether magnetic coupling can lead to SMM behavior, the alternating current magnetic susceptibilities of **1-Ho**, **1-Er**, **1-Tb**, **2-Ho**, **2-Er**, and **2-Tb** were measured (Figures S18−S23, Supporting Information). The in-phase (χ_M') and out-of-phase (χ_M'') signals at low temperatures of **1-Ho**, **1-Er**, **1-Tb**, **2-Ho**, **2-Er**, and **2-Tb** do not exhibit frequency dependence with an increase of the frequency, clearly illustrating the absence of slow relaxation of the magnetization in **1-Ho**, **1-Er**, **1-Tb**, **2-Ho**, **2-Er**, and **2-Tb**, which may be attributed to fast quantum tunneling or the lack of low lying excited levels.[39a] Notably, the alternating current magnetic susceptibilities of **1-Ho**, **1-Er**, **2-Ho**,and **2-Er** are obviously different from those observed in $[Ho(W_5O_{18})_2]^{9-}$ and $[Er(W_5O_{18})_2]^{9-}$,[37b,39b] which may be related to structural parameters of the Ln coordination spheres and weak magnetic couplings within Ln centers mediated by ox^{2-} bridges.

■ CONCLUSIONS

In summary, two kinds of oxalate-bridging tetra-Ln clustersanchored in lacunary Lindqvist isopolytungstates have been prepared and represent rare isopolytungstate construction modes based on polycarboxylate, Ln, and tungsten elements. To our knowledge, **1** represents the first rectangular double-oxalate-bridging tetra-Ln cluster encapsulated divacant Lindqvist isopolyoxotungstate hybrid, and **2** is the first square double-oxalate-bridging tetra-Ln cluster anchored isopolyoxotungstate hybrid. The solid-state photofluorescence spectra of **1-Eu** and **2-Eu** show intense, sharp, and narrow emission bands originating from the characteristic $^5D_0 \rightarrow {}^7F_J$ transitions in the orange visible region, and **1-Tb** and **2-Tb** display the green photofluorescence mainly derived from $^5D_4 \rightarrow {}^7F_5$ transitions. Moreover, their fluorescence lifetimes have been obtained. It should be pointed out that the photoluminescence emissions of **1-Eu**, **2-Eu**, **1-Tb**, and **2-Tb** are derived not only from POM-centered LMCT processes but also oxalate ligands to some degree contributions to their luminescence behavior. Magnetic susceptibility studies of **1** and **2** have been made. The declining of $\chi_M T$ upon cooling for **1** and **2** is mostly related to the progressive thermal depopulation of the excited state of Ln cations. Although there has been recent great focus on single-molecule magnets of Tb^{III} and Dy^{III} complexes because of their significant magnetic anisotropy arising from the largely unquenched orbital angular momentum, no frequency dependence of in-phase signals and the out-of-phase signals is observed for **1-Ho**, **1-Er**, **1-Tb**, **2-Ho**, **2-Er**, and **2-Tb**, which indicates the absence of slow relaxation of the magnetization. Obviously, the high coordination number of oxyphilic Ln ions and the bridging functionality of oxalates are responsible for organic−inorganic hybrid rectangular and square structures of **1** and **2**, which provides the remarkable feasibility for constructing unprecedented gigantic hybrid poly(isopolyoxotungstate) species with special properties. Considering that the electron-conjugated functional organic ligands and POM fragments can be worked as good chromophores to sensitize the luminescence emission of Ln ions and can also tune magnetic interactions with Ln ions, in subsequent work, other multifunctional poly(carboxylic acid) ligands and different POM moieties will be introduced to this system. We believe that the findings herein and afterward will greatly enrich synthetic chemistry and coordination chemistry of isopolyoxotungstates and make it become one of the most appealing areas of modern inorganic chemistry.

■ ASSOCIATED CONTENT

Ⓢ Supporting Information

IR spectra of **1** and **2**, related structure figures, solid-state excitation spectra, and luminescence photographs of **1-Eu**, **2-Eu**, **1-Tb**, and **2-Tb**, relevant magnetic plots of all **1** and **2**, and the CIF files of **1** and **2**. This material is available free of charge via the Internet at http://pubs.acs.org.

■ AUTHOR INFORMATION

Corresponding Authors

*J.Z. E-mail: zhaojunwei@henu.edu.cn. Fax: (+86) 371 23886876.
*Z.W. E-mail: wangzhenling@zknu.edu.cn.
*L.C. E-mail: ljchen@henu.edu.cn.

Notes

The authors declare no competing financial interest.

■ ACKNOWLEDGMENTS

This work was supported by the Natural Science Foundation of China (Grants 21101055, 21301049, and U1304208), China Postdoctoral Science Foundation Funded Project (201104392, 20100470996), the Natural Science Foundation of Henan Province (122300410106, 102300410093), the Foundation of State Key Laboratory of Structural Chemistry (20120013), 2012 Young Backbone Teachers Foundation from Henan Province and the Students Innovative Pilot Plan of Henan University (2012, 2013, 2014).

■ REFERENCES

(1) (a) Marrot, J.; Pilette, M. A.; Haouas, M.; Floquet, S.; Taulelle, F.; López, X.; Poblet, J. M.; Cadot, E. *J. Am. Chem. Soc.* **2012**, *134*, 1724. (b) Zhao, Y.; Deng, D.-S.; Ma, L.-F.; Ji, B.-M.; Wang, L.-Y. *Chem. Commun.* **2013**, *49*, 10299. (c) Heine, J.; Müller-Buschbaum, K. *Chem. Soc. Rev.* **2013**, *42*, 9232. (d) Descalzo, A. B.; Martínez-Mañez, R.; Sancenón, F.; Hoffmann, K.; Rurack, K. *Angew. Chem., Int. Ed.* **2006**, *45*, 5924. (e) Zheng, S.-T.; Zhang, J.; Li, X.-X.; Fang, W.-H.; Yang, G.-Y. *J. Am. Chem. Soc.* **2010**, *132*, 15102.

(2) (a) Mialane, P.; Dolbecq, A.; Sécheresse, F. *Chem. Commun.* **2006**, 3477. (b) Zheng, S.-T.; Yang, G.-Y. *Chem. Soc. Rev.* **2012**, *41*, 7623. (c) Song, Y.-F.; Long, D.-L.; Ritchie, C.; Cronin, L. *Chem. Rec.* **2011**, *11*, 158. (d) Dolbecq, A.; Dumas, E.; Mayer, C. R.; Mialane, P. *Chem. Rev.* **2010**, *110*, 6009. (e) Hirano, T.; Uehara, K.; Uchida, S.; Hibino, M.; Kamata, K.; Mizuno, N. *Inorg. Chem.* **2013**, *52*, 2662. (f) Long, D.-L.; Tsunashima, R.; Cronin, L. *Angew. Chem., Int. Ed.* **2010**, *49*, 1736. (g) Miras, H. N.; Yan, J.; Long, D.-L.; Cronin, L. *Chem. Soc. Rev.* **2012**, *41*, 7403. (h) Oms, O.; Dolbecq, A.; Mialane, P. *Chem. Soc. Rev.* **2012**, *41*, 7497.

(3) Dolbecq, A.; Mialane, P.; Lisnard, L.; Marrot, J.; Sécheresse, F. *Chem.—Eur. J.* **2003**, *9*, 2914.

(4) (a) Mialane, P.; Dolbecq, A.; Rivière, E.; Marrot, J.; Sécheresse, F. *Eur. J. Inorg. Chem.* **2004**, 33. (b) Kortz, U. *J. Cluster Sci.* **2003**, *14*, 205. (c) Zheng, S.-T.; Zhang, J.; Yang, G.-Y. *Angew. Chem., Int. Ed.* **2008**, *47*, 3909. (d) Sun, C.-Y.; Liu, S.-X.; Liang, D.-D.; Shao, K.-Z.; Ren, Y.-H.; Su, Z.-M. *J. Am. Chem. Soc.* **2009**, *131*, 1883. (e) Rodriguez-Albelo, L. M.; Ruiz-Salvador, A. R.; Sampieri, A.; Lewis, D. W.; Gómez, A.; Nohra, B.; Mialane, P.; Marrot, J.; Sécheresse, F.; Mellot-Draznieks, C.; Biboum, R. N.; Keita, B.; Nadjo, L.; Dolbecq, A. *J. Am. Chem. Soc.* **2009**, *131*, 16078. (f) Nohra, B.; Moll, H. E.; Rodriguez Albelo, L. M.; Mialane, P.; Marrot, J.; Mellot-Draznieks, C.; O'Keeffe, M.; Biboum, R. N.; Lemaire, J.; Keita, B.; Nadjo, L.; Dolbecq, A. *J. Am. Chem. Soc.* **2011**, *133*, 13363.

(5) (a) Yamase, T. *Chem. Rev.* **1998**, *98*, 307. (b) Binnemans, K. *Chem. Rev.* **2009**, *109*, 4283. (c) Ritchie, C.; Moore, E. G.; Speldrich, M.; Kögerler, P.; Boskovic, C. *Angew. Chem., Int. Ed.* **2010**, *49*, 7702. (d) Ritchie, C.; Baslon, V.; Moore, E. G.; Reber, C.; Boskovic, C. *Inorg. Chem.* **2012**, *51*, 1142.

(6) (a) Sheldrick, G. M. *SADABS: Program for Empirical Absorption Correction of Area Detector Data*; University of Göttingen: Göttingen, Germany, 1996. (b) Sheldrick, G. M. *SHELXS 97, Program for Crystal Structure Solution*; University of Göttingen: Göttingen, Germany, 1997. (c) Sheldrick, G. M. *SHELXL 97, Program for Crystal Structure Refinement*; University of Göttingen, Germany, 1997.

(7) (a) Peacock, R. D.; Weakley, T. J. R. *J. Chem. Soc. A* **1971**, 1836. (b) Reinoso, S.; Vitoria, P.; Felices, L. S.; Lezama, L.; Gutiérrez-Zorrilla, J. M. *Inorg. Chem.* **2006**, *45*, 108. (c) Zhao, J. W.; Shi, D. Y.; Chen, L. J.; Ma, P. T.; Wang, J. P.; Niu, J. Y. *CrystEngComm* **2011**, *13*, 3462. (d) Zhang, S.; Wang, Y.; Zhao, J.; Ma, P.; Wang, J.; Niu, J. *Dalton Trans.* **2012**, *41*, 3764.

(8) (a) Wassermann, K.; Dickman, M. H.; Pope, M. T. *Angew. Chem., Int. Ed. Engl.* **1997**, *36*, 1445. (b) Ghosh, S.; Datta, S.; Friend, L.; Cardona-Serra, S.; Gaita-Ariño, A.; Coronado, E.; Hill, S. *Dalton Trans.* **2012**, *4*, 13697.

(9) Mialane, P.; Dolbecq, A.; Marrot, J.; Sécheresse, F. *Inorg. Chem. Commun.* **2005**, 503.

(10) (a) Hussain, F.; Bassil, B. S.; Bi, L.-H.; Reicke, M.; Kortz, U. *Angew. Chem., Int. Ed.* **2004**, *43*, 3485. (b) Pichon, C.; Dolbecq, A.; Mialane, P.; Marrot, J.; Rivière, E.; Sécheresse, F. *Dalton Trans.* **2008**, 71.

(11) Sarma, M.; Chatterjee, T.; Das, S. K. *Dalton Trans.* **2011**, *40*, 2954.

(12) (a) Szeto, K. C.; Lillerud, K. P.; Tilset, M.; Bjørgen, M.; Prestipino, C.; Zecchina, A.; Amberti, C.; Bordiga, S. *J. Phys. Chem. B* **2006**, *110*, 21509. (b) Bordiga, S.; Damin, A.; Bonino, F.; Zecchina, A.; Spanò, G.; Rivetti, F.; Bolis, V.; Lamberti, C. *J. Phys. Chem. B* **2002**, *106*, 9892.

(13) Bordiga, S.; Lamberti, C.; Ricchiardi, G.; Regli, L.; Bonino, F.; Damin, A.; Lillerud, K. P.; Bjorgen, M.; Zecchina, A. *Chem. Commun.* **2004**, *40*, 2300.

(14) Zhang, D.; Zhang, S.; Ma, P.; Wang, J.; Niu, J. *Inorg. Chem. Commun.* **2012**, *20*, 191.

(15) (a) Deacon, G. B.; Phillips, R. *Coord. Chem. Rev.* **1980**, *33*, 227. (b) Li, C. H.; Huang, K. L.; Chi, Y. N.; Liu, X.; Han, Z. G.; Shen, L.; Hu, C. W. *Inorg. Chem.* **2009**, *48*, 2010.

(16) (a) Auwer, C. D.; Charbonnel, M. C.; Drew, M. G. B.; Grigoriev, M.; Hudson, M. J.; Iveson, B. P.; Madic, C.; Nierlich, M.; Presson, M. T.; Revel, R.; Russell, M. L.; Thuery, P. *Inorg. Chem.* **2000**, *39*, 1487. (b) Zhang, S.; Zhao, J.; Ma, P.; Niu, J.; Wang, J. *Chem.—Asian J.* **2012**, *7*, 966.

(17) (a) Richardson, F. S. *Chem. Rev.* **1982**, *82*, 541. (b) Pope, S. J. A.; Coe, B. J.; Faulkner, S.; Bichenkova, E. V.; Yu, X.; Douglas, K. T. *J. Am. Chem. Soc.* **2004**, *126*, 9490. (c) Buünzli, J. C. G.; Piguet, C. *Chem. Soc. Rev.* **2005**, *34*, 1048.

(18) Sopasis, G. J.; Orfanoudaki, M.; Zarmpas, P.; Philippidis, A.; Siczek, M.; Lis, T.; O'Brien, J. R.; Milios, C. J. *Inorg. Chem.* **2012**, *51*, 1170.

(19) (a) Chandler, B. D.; Cramb, D. T.; Shimizu, G. K. H. *J. Am. Chem. Soc.* **2006**, *128*, 10403. (b) Mahata, P.; Ramya, K. V.; Natarajan, S. *Chem.—Eur. J.* **2008**, *14*, 5839.

(20) (a) Lill, D. T.; Bettencourt-Dias, A.; Cahill, C. L. *Inorg. Chem.* **2007**, *46*, 3960. (b) Kirby, A. F.; F. Richardson, S. *J. Phys. Chem.* **1983**, *87*, 2544. (c) Stouwdam, J. W.; van Veggel, F. C. J. M. *Nano Lett.* **2002**, *2*, 733. (d) Zhang, T.; Spitz, C.; Antonietti, M.; Faul, C. F. J. *Chem.—Eur. J.* **2005**, *11*, 1001.

(21) (a) Beeby, A.; Clarkson, I. M.; Dickins, R. S.; Faulkner, S.; Parker, D.; Royle, L.; de Sousa, A. S.; Williams, J. A. G.; Woods, M. *J. Chem. Soc., Perkin Trans. 2* **1999**, *3*, 493. (b) Black, C. A.; Costa, J. S.; Fu, W. T.; Massera, C.; Roubeau, O.; Teat, S. J.; Aromí, G.; Gamez, P.; Reedijk, J. *Inorg. Chem.* **2009**, *48*, 1062. (c) Gao, Q.; Wang, X.; Jacobson, A. J. *Inorg. Chem.* **2011**, *50*, 9073. (d) Rosen, D. L.; Niles, S. *Appl. Spectrosc.* **2001**, *55*, 208. (e) Wang, Z. L.; Quan, Z. W.; Jia, P. Y.; Lin, C. K.; Luo, Y.; Chen, Y.; Fang, J.; Zhou, W.; O'Connor, C. J.; Lin, J. *Chem. Mater.* **2006**, *18*, 2030.

(22) (a) de Sá, G. F.; Malta, O. L.; de Mello Donegá, C.; Simas, A. M.; Longo, R. L.; Santa-Cruz, P. A., Jr.; da Silva, E. F. *Coord. Chem. Rev.* **2000**, *196*, 165. (b) Kido, J.; Okamoto, Y. *Chem. Rev.* **2002**, *102*, 2357.

(23) (a) Li, Y.; Zheng, F. K.; Liu, X.; Zou, W. Q.; Guo, G. C.; Lu, C. Z.; Huang, J. S. *Inorg. Chem.* **2006**, *45*, 6308. (b) Ishikawa, N.; Iino, T.;

Kaizu, Y. *J. Am. Chem. Soc.* **2002**, *124*, 11440. (c) Costes, J. P.; Nicodème, F. *Chem.—Eur. J.* **2002**, *8*, 3442.

(24) (a) Kahn, M. L.; Sutter, J.; Golhen, S.; Guionneau, P.; Ouahab, L.; Kahn, O.; Chasseau, D. *J. Am. Chem. Soc.* **2000**, *122*, 3413. (b) Zhao, J. W.; Luo, J.; Chen, L. J.; Yuan, J.; Li, H. Y.; Ma, P. T.; Wang, J. P.; Niu, J. Y. *CrystEngComm* **2012**, *14*, 7981.

(25) Costes, J.-P.; Nicodème, F. *Chem.—Eur. J.* **2002**, *8*, 3442.

(26) Benelli, C.; Gatteschi, D. *Chem. Rev.* **2002**, *102*, 2369.

(27) (a) Furrer, A.; Güdel, H. U.; Krausz, E. R.; Blank, H. *Phys. Rev. Lett.* **1990**, *64*, 68. (b) Costes, J. P.; Dahan, F.; Dupuis, A.; Laurent, J. P. *Chem.—Eur. J.* **1998**, *4*, 1616. (c) Zhang, Z. H.; Okamura, T.; Hasegawa, Y.; Kawaguchi, H.; Kong, L. Y.; Sun, W. Y.; Ueyama, N. *Inorg. Chem.* **2005**, *44*, 6219. (d) Figuerola, A.; Ribas, J.; Llunell, M.; Casanova, D.; Maestro, M.; Alvarez, S.; Diaz, C. *Inorg. Chem.* **2005**, *44*, 6939. (e) Kahn, O. *Molecular Magnetism*; VCH: Weinheim, Germany, 1993.

(28) (a) Clemente-Juan, J. M.; Coronado, E.; Gaita-Ariño, A. *Chem. Soc. Rev.* **2012**, *41*, 7464. (b) Cardona-Serra, S.; Clemente-Juan, J. M.; Coronado, E.; Gaita-Ariño, A.; Camón, A.; Evangelisti, M.; Luis, F.; Martínez-Pérez, M. J.; Sesé, J. *J. Am. Chem. Soc.* **2012**, *134*, 14982. (c) Zhang, P.; Guo, Y.-N.; Tang, J. K. *Coord. Chem. Rev.* **2013**, *257*, 1728. (d) Vonci, M.; Boskovic, C. *Aust. J. Chem.* **2014**, DOI: 10.1071/CH14166. (e) Sorace, L.; Benelli, C.; Gatteschi, D. *Chem. Soc. Rev.* **2011**, *40*, 3092. (f) Woodruff, D. N.; Winpenny, R. E. P.; Layfield, R. A. *Chem. Rev.* **2013**, *113*, 5110.

(29) Liu, R.; Zhao, S.; Xiong, C.; Xu, J.; Li, Q.; Fang, D. *J. Mol. Struct.* **2013**, *1036*, 107.

(30) He, F.; Tong, M. L.; Yu, X. L.; Chen, X. M. *Inorg. Chem.* **2005**, *44*, 559.

(31) Figuerola, A.; Ribas, J.; Casanova, D.; Maestro, M.; Alvarez, S.; Diaz, C. *Inorg. Chem.* **2005**, *44*, 6949.

(32) Nayak, S.; Roubeau, O.; Teat, S. J.; Beavers, C. M.; Gamez, P.; Reedijk, J. *Inorg. Chem.* **2010**, *49*, 216.

(33) (a) Przychodzeń, P.; Pełka, R.; Lewiński, K.; Supel, J.; Rams, M.; Tomala, K.; Sieklucka, B. *Inorg. Chem.* **2007**, *46*, 8924. (b) Campbell, V. E.; Guillot, R.; Riviere, E.; Brun, P.-T.; Wernsdorfer, W.; Mallah, T. *Inorg. Chem.* **2013**, *52*, 5194.

(34) Feng, X.; Zhao, J.; Liu, B.; Wang, L.; Ng, S.; Zhang, G.; Wang, J.; Shi, X.; Liu, Y. *Cryst. Growth Des.* **2010**, *10*, 1399.

(35) (a) Arumuganathan, T.; Das, S. K. *Inorg. Chem.* **2009**, *48*, 496. (b) Lam, A. W. H.; Wong, W.-T.; Wen, G. H.; Zhang, X. X.; Gao, S. *New J. Chem.* **2001**, *25*, 531.

(36) Caneschi, A.; Dei, A.; Gatteschi, D.; Poussereau, S.; Sorace, L. *Dalton Trans.* **2004**, 1048.

(37) (a) Li, Z.; Zhu, G.; Guo, X.; Zhao, X.; Jin, Z.; Qiu, S. *Inorg. Chem.* **2007**, *46*, 5174. (b) AlDamen, M. A.; Cardona-Serra, S.; Clemente-Juan, J. M.; Coronado, E.; Gaita-Ariño, A.; Martí-Gastaldo, C.; Luis, F.; Montero, O. *Inorg. Chem.* **2009**, *48*, 3467.

(38) Díaz-Gallifa, P.; Fabelo, O.; Pasán, J.; Cañadillas-Delgado, L.; Lloret, F.; Julve, M.; Ruiz-Pérez, C. *Inorg. Chem.* **2014**, *53*, 6299.

(39) (a) Sun, Y. G.; Li, J.; Li, K. L.; Xu, Z. H.; Ding, F.; Ren, B. Y.; Wang, S. J.; You, L. X.; Xiong, G.; Smet, P. F. *CrystEngComm* **2014**, *16*, 1777. (b) AlDamen, M. A.; Clemente-Juan, J. M.; Coronado, E.; Martí-Gastaldo, C.; Gaita-Ariño, A. *J. Am. Chem. Soc.* **2008**, *130*, 8874.